JPL PUBLICATION 79-60

Models of P/Tempel 2

Ray L. Newburn, Jr.

(NASA-CR-162292) MODELS OF P/TEMPEL 2 (Jet Propulsion Lab.) 52 p HC A04/MF A01 CSCL 03B
N79-33138
Unclas
G3/91 35783

September 1, 1979

National Aeronautics and
Space Administration

Jet Propulsion Laboratory
California Institute of Technology
Pasadena, California

JPL PUBLICATION 79-60

Models of P/Tempel 2

Ray L. Newburn, Jr.

September 1, 1979

National Aeronautics and
Space Administration

Jet Propulsion Laboratory
California Institute of Technology
Pasadena, California

The research described in this publication was carried out by the Jet Propulsion Laboratory, California Institute of Technology, under NASA Contract No NAS7-100

ACKNOWLEDGMENTS

I would like to thank Fred Whipple and Zdenek Sekanina for permission to quote their unpublished results. I would also like to thank ESA (European Space Authority) for permission to present some of the outline of section II here as well as in reference 8.

PRECEDING PAGE BLANK NOT FILMED

ABSTRACT

Quantitative models of Comet Tempel 2 at various heliocentric distances have been created using a semi-empirical theory which ties gas production rates to the light curve. Physical properties of the nucleus and gas and dust densities are supplied for a nominal case and two extreme cases at each distance, the extreme cases being based upon a "sum-of-negative-tolerances" approach.

PRECEDING PAGE BLANK NOT FILMED

CONTENTS

PRECEDING PAGE BLANK NOT FILMED

I. INTRODUCTION

On July 3, 1873 Wilhelm Tempel discovered his second periodic comet as a faint 9-10th magnitude object moving slowly southeast in the constellation of Cetus (1). Seen in 15 of its 20 perihelion passages since that discovery, P/Tempel 2 has the third shortest period (5.27 years) among known comets (2). Its absolute magnitude is about 9.7 (3), not nearly so bright as P/Halley (mag 5.0) but much brighter than say P/Tuttle-Giacobini-Kresak (mag 11.5 except during outbursts). It is a fairly average short period comet in every physical characteristic. As a possible target for spacecraft rendezvous in the next decade, however, Tempel 2 stands alone in combined accessibility and benign environment, and it even permits flight past Halley enroute, with almost no performance penalty (4). This led to the Halley-Tempel 2 flight being selected as the mission of choice early in 1978 by the NASA Comet Science Working Group (5).

Interest in P/Tempel 2 led to an immediate desire for environmental models to use in mission design studies and for scientific payload evaluation. Unfortunately, as is the case for nearly all periodic comets, modern, quantitative data do not exist for Tempel 2. There are, however, many estimates of the apparent brightness of the object, visual comparisons of its apparent brightness with out-of-focus images of nearby stars of known magnitude. These have been gathered together by Sekanina and plotted in the light-curve shown as Figure 1 (3). There are a few crude uncalibrated spectra, the best being those of Bobrovnikoff taken in 1925 (6). These indicate a rather normal comet, having the usual

bands of CN, C_2, C_3, and CO^+ and a very strong continuum. With only this limited information available, it was necessary to turn to the technique developed originally by Newburn to provide models of P/Halley (7,8). A nominal model so produced was used at JPL and NASA during 1978. A refinement of the constants in the theory led to the models presented here, which have been in use since January 1979.

II. MODELING THEORY AND GAS PRODUCTION

In 1978 a general theory was developed tying a comet's gas production to its visual light curve (7). An outline of that theory was prepared to accompany the published models for P/Halley (8). In order to make this document self-contained, that outline is also presented here with only such minor changes as required to make it appropriate to P/Tempel 2.

Light from the head of a comet has three sources, sunlight reflected from the nucleus, sunlight scattered from dust and grains, and light emitted by the gases, largely by the mechanism of resonance fluorescence. The spectral response of the dark-adapted human eye (the scotopic passband) peaks at about 5060 Å and falls to zero near 4000 Å and 6400 Å (Ref. 11). Within this human filter more than 90 percent of the light from gases is that of resonance fluorescence of the Swan bands of the C_2 molecule. Therefore, since we are dealing with only one gaseous species, it should be possible to relate the visual light curve to the gas production rate of a comet with a minimum of free parameters to be derived from observation.

The only practical approach to the desired result would seem to be a simple photometric equation relating the cometary brightness to the effective cross section for each of the three contributing elements, A the nucleus, B the gas, and C the solids, i.e.,

$$A\phi_n(\alpha) + Bf_1(r) + C\phi_d(\alpha)\ f_2(r) = r^2 10^{0.4\left|m_\odot - [m_1(r) - 5 \log \Delta]\right|} \qquad (1)$$

$m_\odot$ = total visual magnitude of the Sun

m_1 = apparent visual magnitude of the comet

r = heliocentric distance (km)

Δ = geocentric distance (AU)

$f_1(r)$ = functional dependence of C_2 production upon H production

$f_2(r)$ = functional dependence of solids production upon H production

α = phase angle

$\phi_n(\alpha)$ = phase function of the nucleus

$\phi_d(\alpha)$ = phase function of the dust

Equation (1) is written in terms of apparent magnitude m_1 since most available data are in that form. The hydrogen production rate is used as the dependent variable since hydrogen is the dominant element in most comets. Furthermore, hydrogen is indirectly an observable from measurements of the intensity of the Lα resonance line at 1216 Å. Therefore, the B term can be derived from observation. Writing the equation this way contains the assumption that cometary brightness is an instantaneous function of the gas production rate, which can be shown to be a valid approximation in the absence of sporadic outbursts.

Solids are lifted from the nucleus by the aerodynamic drag of escaping gases. Assuming a more or less homogeneously mixed active layer, the solids to gas ratio should remain constant for a few apparitions (barring outbursts), and the mass of solids released should be a constant linear function of the gas production, that is $f_2(r) \propto g(r)$ where $g(r)$ is the hydrogen production rate.

Initially one might assume that the C_2 abundance also maintains a constant mixing ratio relative to the total gas production or hydrogen production. In those cases where appropriate spectrophotometry exists, this is simply not the case (7). The C_2 abundance in fact varies roughly as the square of the hydrogen production. The production mechanism for C_2 is unknown, but it does not appear to be the simple photodissociation production from a parent molecule. Here it is assumed that $f_1(r) \propto g^2(r)$ in agreement with the available observations. The basic photometric equation has now become:

$$A\phi_n(\alpha) + Bg^2(r) + C\phi_d(\alpha)\ g(r) = r^2 10^{0.4\left|m_\odot - [m_1(r) - 5 \log \Delta]\right|} \qquad (2)$$

To zero order, the coefficient of each term might be considered constant. In fact, that is reliably true only for A. The loss mechanism for C_2 is almost certainly photodissociation or photoionization, since the C_2 coma is sufficiently large that molecular interactions can occur only at its very center. The efficiency of loss then should vary inversely as the square of heliocentric distance, with the coma growing in size as the comet moves outward. If the naked eye "sees" to some limiting surface brightness, the fraction of produced C_2 seen also will vary with heliocentric distance. In effect, B is a function of r.

Newburn (7) has shown that for a neutral molecule, in the case where the scale length for loss is much greater than that for creation (whatever the creation mechanism), an excellent approximation for B(r) is given by:

$$B(r) = R \frac{l_o}{v} \left(\frac{r}{r_o}\right)^2 \left[1 - Ki_2\left(\frac{c r_o^2}{l_o r^2}\right)\right] \qquad (3)$$

l_o = scale length for loss of C_2 at 1 AU (km)

v = expansion velocity of C_2

r_o = 149,597,871 km (1 AU)

c = apparent coma radius (km)

Ki_2 = second modified Bessel integral function of the second kind

R = constant of proportionality

In the limit where $c >> r_o^2/l_o r^2$ the quantity $[1 - Ki_2( )] \rightarrow 1$, and the expression for B(r) shows the pure r^2 behavior expected due to the decrease in solar flux. The constant R in effect encompasses two "efficiencies." These are the number of C_2 radicals produced for a given hydrogen production (squared) and the visible light produced per C_2 radical.

The removal mechanism for non-volatile solids, other than expansion at an initial velocity imparted at the nucleus, is radiation pressure. In detail its effectiveness at any given heliocentric distance is a complex function of particle size, shape, and composition, making theoretical evaluation difficult. Radiation pressure decreases as the square of increasing distance from the Sun, and the velocity of ejection from the nucleus also decreases, increasing the density of particles inside a circle at any given distance from the nucleus. At relatively large heliocentric distance $C(r) \propto \sim r^4$. Nearer to the Sun the particles reach a constant velocity equal to the accelerating gas and $C(r) \propto \sim r^2$. Rather than using a complicated theoretical relationship, the decision was made to use an empirical law derived from photometric observations of the continua of other comets of similar continuum strength. This relationship "fortunately" has the proper theoretical form.

The photometric equation has now become

$$A\phi_n(\alpha) + B(r)g^2(r) + C(r)\ \phi_d(\alpha)\ g(r) = r^2 10^{0.4\left[m_\odot - [m_1(r) - 5\ \log\ \Delta]\right]} \tag{4a}$$

with

$$B(r) = R\ \frac{1_o}{v}\left(\frac{r}{r_o}\right)^2\left[1 - Ki_2\left(\frac{cr_o^2}{1_o r^2}\right)\right] \tag{4b}$$

and

$$C(r) = \text{an empirical function} \tag{4c}$$

Defining a ratio $\delta(r)$ as the illuminance from solids divided by the illuminance from gas seen in the scotopic passband means:

$$\delta(r) = \frac{C(r)\ \phi_d(\alpha)\ g(r)}{B(r)\ g^2(r)} \tag{5}$$

and the solution to the photometric equation for g(r) is

$$g^2(r) = \frac{r^2 10^{0.4\left[m_\odot - [m_1(r) - 5\ \log\ \Delta]\right]} - A\ \phi_n(d)}{B(r)\ [1 + \delta(r)]} \tag{6}$$

The graph of $\delta(r)$ for comets of continuum strength comparable to P/Tempel 2 is given as Figure 2 taken from Newburn (7). Both Tempel 2 and Encke are old, very short period comets with cone-shaped comae, so the value selected for R in the nominal model was 4×10^{-59} $(km^2\ mol^{-1})$ $(mol\ s^{-1})^{-1}$, the value derived for P/Encke from observation. One could rationally argue that a more standard value, similar to that derived from

comets such as Bennett and West, should be used instead. They after all have strong continua similar to Tempel 2. Until the mechanism by which C_2 is formed is understood, whether its relative abundance to H is dependent in any way upon distributed solids, dependent just upon the abundance of one or more parent molecules, or dependent upon cometary age, etc. the choice will be rather arbitrary. Extreme models were produced using $R = 1 \times 10^{-58}$ and $R = 1 \times 10^{-62}$. Since $g \propto R^{-1/2}$, this implies a range of two orders of magnitude in the actual hydrogen abundance derived. The range selected does encompass the average value for bright comets ($\sim 3 \times 10^{-61}$) and a comparable opposite extreme which is larger than <u>any</u> observed value.

The coefficient A for the nucleus contribution is just equal to pR^2, where p is the geometric albedo and R the nucleus radius. For most short-period comets the value of A is ~ 1 km^2, so in fact the term can be ignored except at very large heliocentric distances. At very large distances, of course, the gas production falls to zero, and what remains is just the photometric expression for the reflection from a bare nucleus, namely

$$A\phi_n(\alpha) = pR^2\,\phi_n(\alpha) = r^2 10^{0.4\left[m_\odot - m_1(r) - 5\log\Delta\right]} \qquad (7)$$

The hydrogen production figures for P/Tempel 2 resulting from this semi-empirical approach are given in Table 1. It is assumed that this hydrogen is entirely derived from the dissociation of H_2O, two hydrogen atoms from each water molecule. Since Tempel 2 is a very old comet in an orbit with only 4.69 AU aphelion distance, parent species more volatile than water should be limited to no more than a small number of small molecules which can be trapped in the water lattice. While the non-gravitational

effects upon the orbit of P/Tempel 2 are small, they exist and are completely consistent with water as the dominant outgassing species (9). Therefore while there are very probably other small sources of H than H_2O, and there must be sources of the observed C_2, CN, etc., they can be modeled as a 10 percent addition to the water.

i.e. $N(H_2O) = 0.5\ N(H)$

$N(\text{other}) = 0.1\ N(H_2O)$

$N(\text{all gas}) = 0.55\ N(H)$

The total gas production given in Table 2 for the nominal model is just this value of 55% of the derived H production in Table 1. The extreme models are derived assuming pure water (50% of the H production) and 20% other gases (60% of the H production).

III. PROPERTIES OF THE NUCLEUS

The properties of the P/Tempel 2 nucleus derived or assumed in these models are given in Table 3. Lacking direct measurements of the nucleus, its size has been evaluated photometrically by means of equation 7. In 1978 Sekanina gathered together all of Roemer's approximate photographic magnitudes for Tempel 2 at large heliocentric distances (10). Assuming a geometric albedo of 0.15, these suggested a radius of 1500 meters. An extremely low albedo of 0.03 would increase the radius to 3500 meters, while a high albedo of 0.5 plus the assumption that half the apparent brightness was still coma at 2.7 AU resulted in a radius of 250 meters. Since that time, accurate photoelectric measurements of Tempel 2 at similar distances have suggested an albedo of 0.15 and a radius of 1600 m (11). This is quite close to the adopted nominal value, and change of the values in use seems unwarranted.

Since its conception by Whipple (12, 13) the icy conglomerate nucleus has been pictured as an ill consolidated, poorly conducting ball of frozen gases. A fresh comet then might have a bulk density somewhat less than 1 g cm^{-3}, while a very old, largely degassed, but still poorly consolidated comet might approach the density of primitive solids. Lacking real knowledge, an almost traditional 1 g cm^{-3} is used nominally. The mass quoted is simply the product of density and volume, and the escape velocity is $(2GM/R)^{1/2}$.

Whipple's recently developed "zero date method" for determination of nucleus rotation periods (14) has been applied to Tempel 2, but with difficulty because of lack of data. Whipple's tentative best value is that given for the nominal model, but he states the period could be twice the listed value or a value considerably different (15). The extreme low period is roughly that at which an ice sphere would disrupt. Large lag angles between the subsolar point and maximum activity (3) suggest that the period cannot be very long, so 24 hours seems a conservative, if uncertain, upper limit.

The mean molecular masses result from the assumption that the molecules "other" than water (18 amu) discussed at the end of section II have a mean molecular mass of 44 amu. Thus the nominal mean molecular mass is

$$\frac{18 + 0.1 \times 44}{1.1} = 20.4 \text{ amu}$$

Bright, long-period comets typically exhibit nearly spherical comae as seen in the light of neutral molecules and have their photometric center of brightness centered in the sphere. Sekanina has found that old,

short-period comets typically exhibit comae which are fan-shaped in cross section, extending generally sunward from a center of brightness near the apex. Tempel 2 is such a comet, apparently having a full cone angle of about 60°. This would seem to imply the nucleus is no longer uniformly active, major degassing being confined perhaps to roughly the region of the surface cut by a 60° cone. The nominal gas fluxes of Table 4 then are simply the gas output of the nominal model divided by the area of a 60° cone cutting a 1500-m radius sphere. The extreme low flux was obtained by assuming the extreme low production came isotropically from the largest possible nucleus. The extreme high flow could not be obtained even isotropically from the smallest nucleus without assuming the heat of sublimation to be much smaller than that of water (< 12 kcal $mole^{-1}$). Therefore the extreme high flux is calculated as that from a normal blackbody with a mean heat of sublimation of 11 kcal $mole^{-1}$. At perihelion this is roughly equivalent to the high production rate from a 120° cone on the nominal size of nucleus.

The mass flow ratio of solids to gases enters all dust calculations (see section IV) as a direct multiplier. Values are reported in the literature for two comets with strong continua, Finson and Probstein finding 1.4 for Arend-Roland (16) and Sekanina and Miller 0.5 for Bennett (17). The Bennett number is very likely the better determined, since there are independent gas production measurements for it. Tempel 2 has a very strong continuum, however, and while conversion from ill-determined light fluxes to gas fluxes requires several assumptions, a somewhat larger number than that for Bennett is suggested. Very new work by Sekanina indicates that the particle

size distribution function used for Bennett (and here) may cut off a bit too steeply at the high mass end (as d^{-5} rather than a more appropriate $d^{-4.2}$), which would imply the presence of some additional "hidden" mass (18). In any event the "round number" 1.0 was used here for the nominal dust to gas mass flow ratio. The extreme values of 0.2 and 4.0 seemed reasonable from experience with many model studies. (There was no completely objective way to pick them given the present lack of actual observations.)

With only a small part of the nucleus surface still active, the nominal geometric albedo must be lower than that for even dirty ice. The value selected 0.15 is appropriate for moderately dark asteroidal type bodies. An albedo of 0.03 is near the lower limit for known bodies, while 0.5 is roughly that for the most highly reflective asteroid. The phase function is that used by Sekanina (19).

A solution of the energy balance equation near 1.5 AU will give about 185 K for reasonable choices of Bond albedo, opacity, emissivity, conductivity, and composition. In a bright comet where the temperature is essentially buffered by the sublimation, the temperature remains near 200 K over a wide range of heliocentric distance. For Tempel 2 this is probably not the case, and the temperature may drop by up to 30% at 2.5 AU, but the temperature is used only to determine the gas velocity at the nucleus surface (where it enters only as the square root), so a constant value of 185 K was used for the calculations.

IV. THE DUST PARAMETERS

The mechanism by which dust is removed from a cometary nucleus is aerodynamic entrainment by the outflowing gas. Probstein treated the problem as one of a two-component (dust-gas) fluid expanding to a vacuum, idealizing the force on the dust as the drag on spherical particles (20). Delsemme and Miller used Probstein's results to supply convenient graphs and equations for the terminal velocity of the dust both with and without consideration of gravitational retardation by the nucleus (21). This terminal velocity is virtually reached within about 10 nuclear radii, so practical calculations can be made by considering the dust to expand isotropically from the nucleus with a constant velocity equal to the terminal velocity. These velocities are given for four heliocentric distances in Tables 5-8.

The distribution of dust particle sizes used in these models is given in Table 9. A theory for determination of such a distribution from observations was originally developed by Finson and Probstein and applied to Comet Arend-Roland (16). The function used here was derived for C/Bennett by Sekanina and Miller (17) and has often been used in comet models because it is a bit simpler than the Arend-Roland function, although essentially equivalent. Actually the largest and smallest particles are poorly determined in these observations. Sekanina's latest work based upon observations of anti-tails, which are entirely large particles, indicates that the function should follow $\sim a^{-4.2}$ rather than a^{-5} for the largest sizes (18). These largest particles are sufficiently few in number that the change is relatively unimportant. It will be made when an accumulation of such improvements warrants recalculation of the dust tables.

The dust tables presented here all assume a bulk particle density of 1 g cm^{-3}. The actual variable in a Finson-Probstein analysis is $a = \rho d$, the product of density and diameter. Anyone wishing to use a different density must realize that either the diameter or the number per gram in each class will also change.

The Sekanina-Miller distribution function as given in Table 9 is classified (histogram) data normalized to one gram of dust. The intervals given in the second column are symmetric about the diameters given in the first column. They are uneven in order to match the incommensurable break points in the distribution function and originally for convenience in calculation. For some purposes decades of mass make a more convenient classification. Table 10 presents the distribution function in this form with only the smallest mass interval an irregular one.

The total number of dust particles emitted in each category requires multiplying the distribution function by the number of grams of dust produced.

$$Q_{d_i} = Q\bar{m}Mn(a_i)\Delta a_i \tag{9}$$

Q_{d_i} = number of dust particles produced per second in category i

Q = total gas production (molecules s^{-1})

$\bar{m}$ = mean molecular mass of gas (g $molecule^{-1}$)

M = ratio of dust and gas mass flow rates

$n(a_i)\Delta a_i$ = normalized distribution function

This distribution function was obtained from an active comet close to the Sun. As the gas flow rate drops at larger heliocentric distances, the larger particles can no longer be lifted and remain behind on the surface

of the nucleus. The intrinsic distribution function does not change, but the actual mass flow of solids becomes somewhat less than $Q\bar{m}M$, the mass multiplier of the distribution function. In time this should skew the distribution of remaining material in an old comet somewhat toward larger sizes. Since most of the mass is in small particles and there is no observational data to indicate any substantial effect, this possibility is ignored. The dust produced at four different heliocentric distances is given in Tables 11-14.

Tables 15-18 are calculated in a straightforward manner using the assumption of isotropic expansion from the nucleus.

$$\text{Particle density} = \frac{Q_d}{4\pi R^2 vf} \tag{10}$$

$$\text{Particle flux} = \frac{Q_d}{4\pi R^2 f} \tag{11}$$

Q_d = dust production rate (Tables 11-14)

v = dust velocity (Tables 5-8)

R = distance from nucleus

f = fraction of surface that is active

Actually as the dust flows outward it is acted upon by solar radiation pressure. Its initially linear path becomes one branch of a parabola in comet centered coordinates, the distance to the parabola apex being a function of particle size, initial velocity, and the radiation pressure efficiency coefficient Q_{pr}, while Q_{pr} is itself a function of particle size, shape, and composition (22, 23, 24).

The envelope of the individual parabolic trajectories for particles of a given size is itself a parabola with its vertex on the sun-line at an apex distance E given by

$$E = \frac{v^2 a r^2}{1.388 \times 10^{-4} Q_{pr}} \qquad (12)$$

E = apex distance (cm)

v = terminal velocity (cm s^{-1})

r = heliocentric distance (AU)

Q_{pr} = radiation pressure efficiency

Tables 19-22 give values for E calculated using Q_{pr} = 1.0 for the nominal case, 2.0 for the low model, and 0.5 for the high model. In a steady-state condition (no outbursts) a space probe flying outside this parabolic envelope should be in a hazard-free region so far as encountering debris from the comet's current activity.

Inside the dust envelope particles more than about half way to their vertices can no longer be treated as expanding isotropically from the nucleus. A proper calculation requires taking a particle in each size category with its initial velocity and "launch azimuth," letting it move under the influence of radiation pressure, and then summing over all sizes and launch azimuths for each location in coordinate space. Divine has actually carried out the messy algebra involved in such a computation so it can be programmed for numerical results when necessary (25). Meanwhile Hanner is working on the problem of more realistic values for Q_{pr} (26).

It is important to note that particles launched toward the Sun reverse their solar radial velocity component and travel back through the coma, so a space probe which enters the dust coma will receive some hits from

the anti-nucleus hemisphere. The number will be relatively small, however, since the velocity component perpendicular to the sun-line continually spreads them out.

The calculation just discussed, carried out in comet centered coordinates, is exact only to second order in a time expansion where unit time is 58.132 days. In other words, large, slow-moving particles taking a significant fraction of 58 days to reach the apex of their trajectories are poorly described by such calculations. Similarly even small particles a large distance from the nucleus are not well described. The dust tail of a comet is clearly not parabolic in shape. These calculations should be made in this way only for the sunward hemisphere of a dust coma.

V. ADDITIONAL MODEL PARAMETERS

The parameter most often sought among those not yet discussed is the gas density or pressure at some distance from the nucleus. For H_2O, which is the dominant molecule in these models, it can easily be supplied. The number density n(R) of molecules at a distance R from the nucleus is given by

$$n(R) = \frac{Q_{H_2O}}{4\pi R^2 v} e^{-\frac{R}{\tau_o r^2 v}} \qquad (13)$$

Q_{H_2O} = H_2O production rate (half the hydrogen production rate given in Table 1)

R = distance from nucleus

v = expansion velocity (see paragraphs below)

τ_o = lifetime for photodissociation at 1 AU = 2 x 10^4 s

r = heliocentric distance in AU

assuming photodissociation is the dominant loss mechanism and gas expansion is isotropic.

The velocity at which subliming gas moves radially away from the nucleus is a function of the temperature and the nature of the emitting surface. Delsemme and Miller argue 60% of the mean thermal velocity to be a reasonable value for radial efflux from snow. For very deep narrow pores in an old nucleus this might rise to 66%, but the 60% value was used in calculating the tables in this document. Expanding into a vacuum, some internal energy of the molecules is converted into kinetic energy, and eventually they reach a radial velocity v_∞ near 180% of their initial thermal velocity after all collisional interactions cease (21). This idealized picture assumes there are sufficient collisions to de-excite the molecular rotational states and that various sources of hot ions and electrons are not available to interact with the water molecules.

With no data actually available for Tempel 2, calculations of H_2O number density have been made assuming a radial efflux velocity of 0.6 $\bar{v}$ at the surface, 1.05 at 100 km, 1.25 at 200 km, 1.6 at 500 km, and 1.8 at 1000 km and beyond where $\bar{v}$ is the surface thermal velocity. The assumption is rather arbitrary but certainly results in correct orders of magnitude for the water densities.

If the observed flux of water is produced from a limited area rather than the entire nucleus, then that fractional area must also appear in the denominator of equation 13, at least at the surface. The surface area cut by a 60° cone is 0.067 of the full sphere, raising the surface density by almost a factor of 15 in the nominal models.

If Tempel 2 were a sufficiently active comet with a large molecular collision zone, then that collision zone would act as a large isotropic source as seen from the outside, whatever the actual source. It is a fact, however, that the gas coma of Tempel 2 appears cone shaped, and while some collisionally induced diffusion to the sides must occur, it is modeled here with the factor 0.067 in the denominator. Results of the water density calculations are given in Table 23.

If needed, pressure can be calculated from

$$P = nkT \qquad (14)$$

P = pressure (dynes cm^{-2})

n = n(R) from (13) (cm^{-3})

k = Boltzmann's const. (1.38×10^{-16} ergs deg^{-1})

T = temperature (K)

The temperature T is the kinetic temperature, which is 185 K at the surface of the nucleus and rises to 600 K at 10^3 km and beyond.

Similar results could be tabulated for any parent molecule with a known production rate. Unfortunately HCN and CH_3CN are the only other probable parent molecules observed in any comet, and their production rates are poorly known even for the comets in which they were observed. Water certainly is the dominant species in the inner coma in any event, so the partial pressure of water is very nearly the total pressure, which is of concern to those designing instruments with open filaments, etc.

Most chemical species actually observed in comets are free radicals or ions which are clearly the product of photo and/or chemical processes

in the coma, details largely unknown. Quantitative observations of some of these, especially CN, C_2, and C_3, have been made on a number of comets in recent years. Abundances and photometric models in and of the gaseous coma can be constructed on the basis of such work, but no observations exist for P/Tempel 2. Observations are planned for the 1983 apparition. Meanwhile semi-empirical photometric modeling is planned by analogy with observed comets and will be reported at a later time.

REFERENCES

1. Vsekhsvyatskii, S. K., "Physical Characteristics of Comets," NASA TT F-80, Washington, D.C., 1964.

2. Marsden, B. G., "Catalog of Cometary Orbits, 3rd Edition," Smithsonian Astrophys. Obs., Cambridge, 1979.

3. Sekanina, Z., "Fan-Shaped Coma, Orientation of Rotation Axis, and Surface Structure of a Cometary Nucleus. I. Test of a Model on Four Comets," Icarcus, 37, 420, 1979.

4. Atkins, K. L., "Missions to Comets: An Options Review," Pub. 78-55, Jet Propulsion Laboratory, Pasadena, 1978.

5. "Report of the Comet Science Working Group," TM 80543, National Aeronautics and Space Administration, Washington, D.C., June 1979.

6. Bobrovnikoff, N.T., "On the Spectra of Comets," Astrophys. J., 66, 439-464, 1927.

7. Newburn, R. L. Jr., "Physical Modeling of a Comet from Minimal Data," to be published.

8. Newburn, R. L. Jr., "Physical Models of Comet Halley Based upon Qualitative Data from the 1910 Apparition,: in "The Comet Halley Micrometeroroid Hazard Workshop Proceedings" European Space Authority, 1979.

9. Yeomans, D. K., "Comet Tempel 2 Orbit, Ephemerides and Error Analysis," Pub. 78-85, Jet Propulsion Laboratory, Pasadena, Sept. 1978.

10. Sekanina, Z., "A Report of Encke/Tempel 2 Subgroup to the Comet Science Working Group," Pasadena, March 1978 (private communication).

11. Spinrad, H., Stauffer, J., and Newburn, R. L. Jr., "Optical Spectrophotometry of Comet Tempel 2 Far from the Sun," Pub. Astron. Soc. Pacific (in press) 1979.

12. Whipple, F. L., "A Comet Model. I. The Acceleration of Comet Encke," Astrophys. J. 111, 375-394, 1950.

13. Whipple, F. L., "A Comet Model. II. Physical Relations for Comets and Meteors," Astrophys. J., 113, 464-474, 1951.

14. Whipple, F. L., "Rotation Period for Comet Donati," Nature, 273, 134-135, 1978.

15. Whipple, F. L., private communication, 1978.

16. Finson, M. L. and Probstein, R. F., "A Theory of Dust Comets. II. Results for Comet Arend-Roland," Astrophys. J., 154, 353-380, 1968.

REFERENCES (continued)

17. Sekanina, Z., and Miller, F. D., "Comet Bennett 1970 II," Science, 179, 565-567, 1973.

18. Sekanina, Z., "Expected Characteristics of Large Dust Particles in Periodic Comet Halley," in "The Comet Halley Micrometeoroid Hazard Workshop Proceedings," European Space Authority, 1979.

19. Sekanina, Z., "A Continuing Controversy: Has the Cometary Nucleus Been Resolved?", 537-585 in "The Study of Comets," ed. B. Donn et al., NASA SP-393, Washington, D.C., 1976.

20. Probstein, R. F., "The Dusty Gas-dynamics of Comet Heads," in "Problems of Hydrodynamics and Continuum Mechanics," 568-583, SIAM, Philadelphia, 1969.

21. Delsemms, A. H., and Miller, D. C., "Physico-Chemical Phenomena in Comets - III. The Continuum of Comet Burnham," Planet. Space Sci. 19, 1229-1257, 1971.

22. Bobrovnikoff, N. T., "Comets," 302-356 in "Astrophysics," J. A. Hynck, New York, 1951.

23. Wurm, K., "The Physics of Comets," 573-617 in "The Moon Meteorites and Comets," "The Solar System, Vol. IV," eds. B. M. Middlehurst and G. P. Kuiper, University of Chicago Press, Chicago, 1962.

24. Greenberg, J. M., "Interstellar Grains," Chap. 6 in "Nebulae and Interstellar Matter," ed. B. M. Middlehurst and L. H. Aller, University of Chicago Press, Chicago, 1968.

25. Divine, N., 1979 (private communication).

26. Hanner, M., 1979 (private communication).

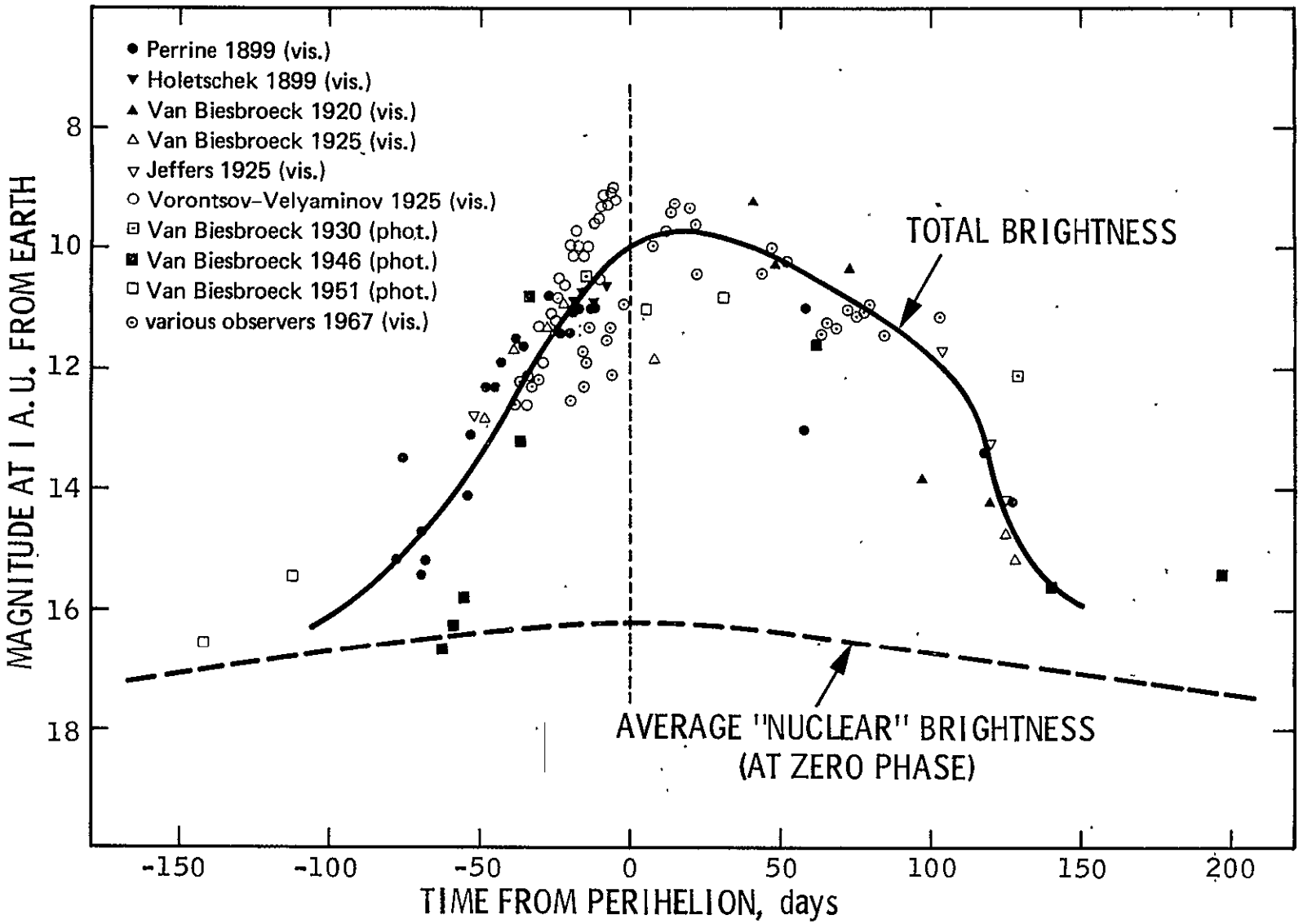

Figure 1. Light curve for P/Tempel 2, from Sekanina (3).

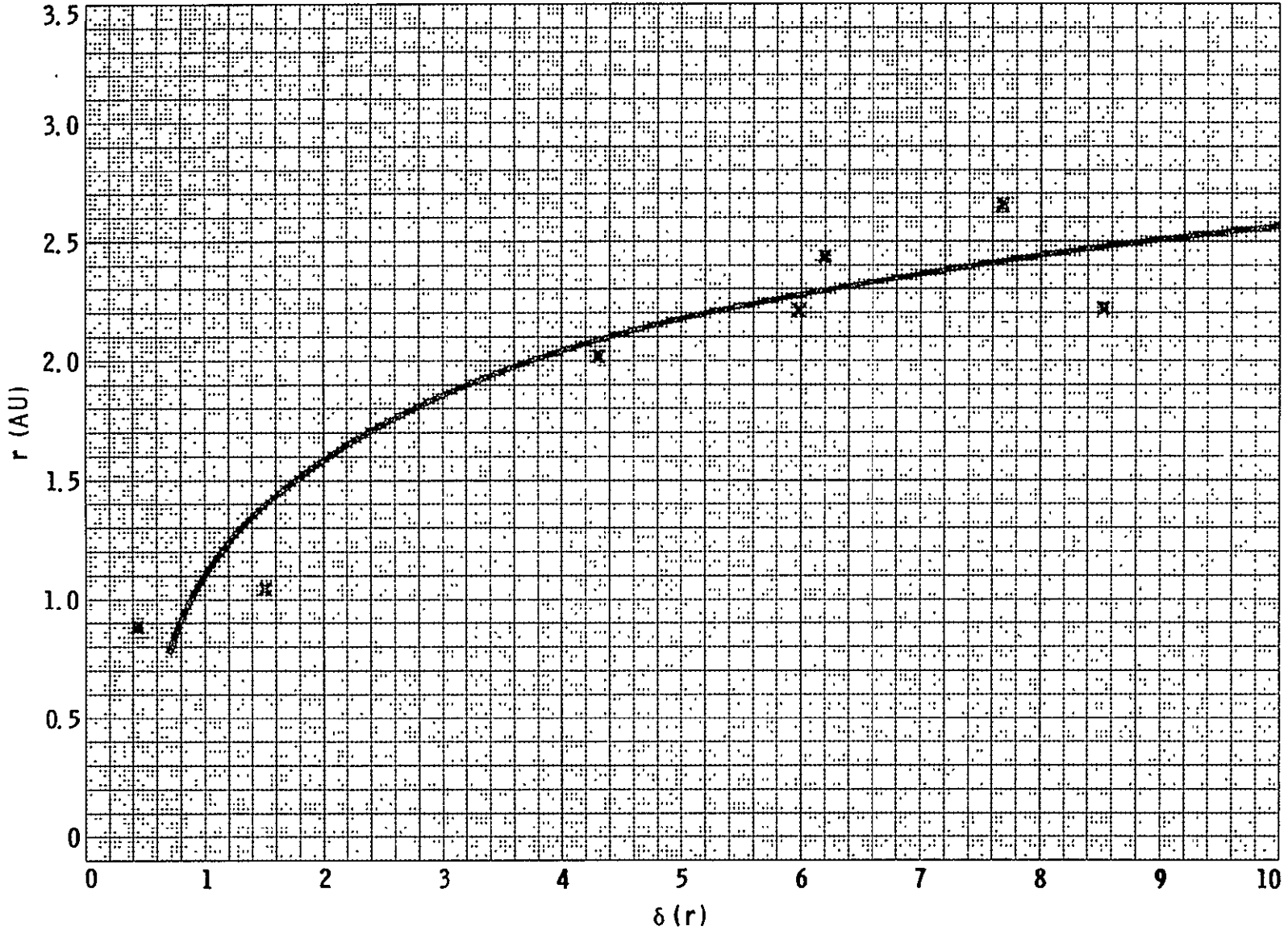

Figure 2. The empirical function δ(r) for comets with very strong continua, from Newburn (7). r is heliocentric distance.

Table 1

P/Tempel 2 Hydrogen Production

Heliocentric Distance (AU)	Production Rate (atoms s^{-1}) Extreme Low	Nominal	Extreme High
Pre-perihelion			
1.6	8.28×10^{25}	1.31×10^{26}	8.28×10^{27}
1.5	1.67×10^{26}	2.64×10^{26}	1.67×10^{28}
1.4	6.45×10^{26}	1.02×10^{27}	6.45×10^{28}
Perihelion 1.37	1.09×10^{27}	1.73×10^{27}	1.09×10^{29}
Post-perihelion			
1.4	1.22×10^{27}	1.93×10^{27}	1.22×10^{29}
1.5	8.51×10^{26}	1.35×10^{27}	8.51×10^{28}
1.6	6.23×10^{26}	9.84×10^{26}	6.23×10^{28}
1.7	4.34×10^{26}	6.86×10^{26}	4.34×10^{28}
1.8	2.76×10^{26}	4.36×10^{26}	2.76×10^{28}
1.9	9.42×10^{25}	1.49×10^{26}	9.42×10^{27}
2.0	5.22×10^{25}	8.25×10^{25}	5.22×10^{27}
2.2	3.24×10^{25}	5.12×10^{25}	3.24×10^{27}

Table 2

P/Tempel 2 Total Gas Production

Heliocentric Distance (AU)	Production Rate, Q (molecules s^{-1}) Extreme Low	Nominal	Extreme High
Pre-perihelion			
1.6	4.14×10^{25}	7.20×10^{25}	4.97×10^{27}
1.5	8.35×10^{25}	1.45×10^{26}	1.00×10^{28}
1.4	3.22×10^{26}	5.61×10^{26}	3.87×10^{28}
Perihelion 1.37	5.45×10^{26}	9.52×10^{26}	6.54×10^{28}
Post-perihelion			
1.4	6.10×10^{26}	1.06×10^{27}	7.32×10^{28}
1.5	4.26×10^{26}	7.42×10^{26}	5.11×10^{28}
1.6	3.12×10^{26}	5.41×10^{26}	3.74×10^{28}
1.7	2.17×10^{26}	3.77×10^{26}	2.60×10^{28}
1.8	1.38×10^{26}	2.40×10^{26}	1.66×10^{28}
1.9	4.71×10^{25}	8.20×10^{25}	5.65×10^{27}
2.0	2.61×10^{25}	4.54×10^{25}	3.13×10^{27}
2.2	1.62×10^{25}	2.82×10^{25}	1.94×10^{27}

Table 3

P/Tempel 2 Physical Properties of Nucleus

Quantity	Extreme Low	Nominal	Extreme High
Radius (m)	250	1500	3500
Mean Bulk Density (g cm^{-3})	0.3	1.0	3.0
Mass (g)	2.0×10^{13}	1.4×10^{16}	5.4×10^{17}
Escape Velocity† (cm s^{-1})	10.3	112	454
Rotation Period (h)	3.0	5.9**	24?
Mean Molecular Mass (amu)‡	18.0	20.4	22.3
Gas Flux*	--	60° cone	isotropic
$\dot{M}$ solids/$\dot{M}$ gas	0.2	1.0	4.0
Geometric Albedo@	0.5	0.15	0.03
Phase Function	$\phi(\alpha) = 0.035\ \alpha$ magnitudes (phase angle α in degrees)		
Temperature (K)#	All calculations assume a value of 185.		

†not including rotational effect (centrifugal term)
**Whipple's tentative value
‡of escaping gas
@high albedo must go with low radius
*isotropic flow from largest nucleus of smallest gas production gives extreme low flux
#see text

Table 4

P/Tempel 2 Surface Gas Flux

Heliocentric Distance (AU)	Flux (molecules $cm^{-2}s^{-1}$) Extreme Low* (isotropic)	Nominal (60° cone)	Extreme High# (black body)
Pre-perihelion			
1.6	2.69×10^{13}	3.80×10^{15}	6.91×10^{17}
1.5	5.42×10^{13}	7.65×10^{15}	7.87×10^{17}
1.4	2.09×10^{14}	2.96×10^{16}	9.03×10^{17}
Perihelion 1.37	3.54×10^{14}	5.03×10^{16}	9.43×10^{17}
Post-perihelion			
1.4	3.96×10^{14}	5.60×10^{16}	9.03×10^{17}
1.5	2.77×10^{14}	3.92×10^{16}	7.87×10^{17}
1.6	2.03×10^{14}	2.86×10^{16}	6.91×10^{17}
1.7	1.41×10^{14}	1.99×10^{16}	6.12×10^{17}
1.8	8.96×10^{13}	1.27×10^{16}	5.46×10^{17}
1.9	3.06×10^{13}	4.33×10^{15}	4.90×10^{17}
2.0	1.70×10^{13}	2.40×10^{15}	4.43×10^{17}
2.2	1.05×10^{13}	1.49×10^{15}	3.66×10^{17}

*Low production isotropically from largest possible nucleus

see text

Table 5

P/Tempel 2 Dust Terminal Velocity Including Gravity
at 1.6AU Pre-perihelion

Particle Diameter (cm)	Velocity ($m\ s^{-1}$) Low Flux	Nominal Flux	High Flux
0.925×10^{-4}	1.89	93.6	395
0.975×10^{-4}	1.57	91.1	386
1.125×10^{-4}	0.72	84.6	377
1.500×10^{-4}	--	72.9	351
2.175×10^{-4}	--	60.1	328
3.3×10^{-4}	--	48.3	295
5.0×10^{-4}	--	38.7	272
9.0×10^{-4}	--	28.2	248
2.4×10^{-3}	--	16.2	179
4.7×10^{-3}	--	10.8	141
6.9×10^{-3}	--	8.5	129
1.0×10^{-2}	--	6.6	114
2.0×10^{-2}	--	3.9	85.6
5.0×10^{-2}	--	1.5	53.2
1.2×10^{-1}	--	0.01	33.4
2.5×10^{-1}	--	--	22.3
5.0×10^{-1}	--	--	15.0
1.0×10^{0}	--	--	9.8
3.1×10^{0}	--	--	4.4
1.0×10^{1}	--	--	1.3

Table 6

P/Tempel 2 Dust Terminal Velocity Including Gravity at 1.4AU Post-perihelion

Particle Diameter (cm)	Velocity (ms^{-1}) Low Flux	Nominal Flux	High Flux
0.925×10^{-4}	37.8	284	404
0.975×10^{-4}	36.5	278	394
1.125×10^{-4}	33.2	263	385
1.500×10^{-4}	27.3	242	377
2.175×10^{-4}	20.9	205	351
3.3×10^{-4}	14.9	179	320
5.0×10^{-4}	10.1	151	292
9.0×10^{-4}	4.8	118	260
2.4×10^{-3}	--	70	201
4.7×10^{-3}	--	49.2	163
6.9×10^{-3}	--	40.1	138
1.0×10^{-2}	--	32.8	120
2.0×10^{-2}	--	22.4	98
5.0×10^{-2}	--	13.2	61.1
1.2×10^{-1}	--	7.6	38.5
2.5×10^{-1}	--	4.4	25.8
5.0×10^{-1}	--	2.4	17.5
1.0×10^{0}	--	0.9	11.6
3.1×10^{0}	--	--	5.4
1.0×10^{1}	--	--	1.8
2.0×10^{1}	--	--	0.5

Table 7

P/Tempel 2 Dust Terminal Velocity Including Gravity at 1.8AU Post-perihelion

Particle Diameter (cm)	Velocity ($m\ s^{-1}$) Low Flux	Nominal Flux	High Flux
0.925×10^{-4}	12.3	173	377
0.975×10^{-4}	11.7	168	372
1.125×10^{-4}	10.2	157	364
1.500×10^{-4}	7.4	135	336
2.175×10^{-4}	4.3	112	320
3.3×10^{-4}	1.5	90.5	295
5.0×10^{-4}	--	73.0	269
9.0×10^{-4}	--	53.7	231
2.4×10^{-3}	--	31.9	167
4.7×10^{-3}	--	22.0	129
6.9×10^{-3}	--	17.7	115
1.0×10^{-2}	--	14.2	99
2.0×10^{-2}	--	9.3	75.8
5.0×10^{-2}	--	4.9	46.9
1.2×10^{-1}	--	2.2	29.3
2.5×10^{-1}	--	0.7	19.5
5.0×10^{-1}	--	--	13.0
1.0×10^{0}	--	--	8.4
3.1×10^{0}	--	--	3.6
1.0×10^{1}	--	--	0.8

Table 8

P/Tempel 2 Dust Terminal Velocity Including Gravity at 2.2AU Post-perihelion

Particle Diameter (cm)	Velocity (ms^{-1}) Low Flux	Nominal Flux	High Flux
0.925×10^{-4}	--	57.6	347
0.975×10^{-4}	--	56.0	343
1.125×10^{-4}	--	52.0	332
1.500×10^{-4}	--	44.6	320
2.175×10^{-4}	--	36.6	295
3.3×10^{-4}	--	29.2	269
5.0×10^{-4}	--	23.2	247
9.0×10^{-4}	--	16.6	203
2.4×10^{-3}	--	9.1	148
4.7×10^{-3}	--	5.8	117
6.9×10^{-3}	--	4.3	100
1.0×10^{-2}	--	3.1	88.2
2.0×10^{-2}	--	1.4	61.6
5.0×10^{-2}	--	--	37.9
1.2×10^{-1}	--	--	23.5
2.5×10^{-1}	--	--	15.5
5.0×10^{-1}	--	--	10.2
1.0×10^{0}	--	--	6.4
3.1×10^{0}	--	--	2.5
1.0×10^{1}	--	--	0.2

Table 9

Sekanina-Miller Distribution Function

Particle Diameter* a (cm)	Interval* Δa (cm)	Normalized Distribution Function $n(a)(cm^{-1}g^{-1})$	Normalized Distribution $n(a)\Delta a$ $(\#g^{-1})$
0.925×10^{-4}	5×10^{-6}		1.27×10^{9}
0.975×10^{-4}	5×10^{-6}		2.94×10^{9}
1.125×10^{-4}	2.5×10^{-5}	$\frac{0.69\cdot(a-0.9\times10^{-4})}{a^5}$	4.31×10^{10}
1.5×10^{-4}	5×10^{-5}		2.73×10^{10}
2.175×10^{-4}	8.5×10^{-5}		1.66×10^{10}
3.3×10^{-4}	1.4×10^{-4}		5.31×10^{9}
5×10^{-4}	2×10^{-4}	$0.45\ a^{-4}$	1.44×10^{9}
9×10^{-4}	6×10^{-4}		4.11×10^{8}
2.4×10^{-3}	2.4×10^{-3}		3.26×10^{7}
4.7×10^{-3}	2.2×10^{-3}		1.55×10^{6}
6.9×10^{-3}	2.2×10^{-3}		2.28×10^{5}
1.0×10^{-2}	4.0×10^{-3}		6.48×10^{4}
2.0×10^{-2}	1.6×10^{-2}		8.10×10^{3}
5.0×10^{-2}	4.4×10^{-2}		2.28×10^{2}
1.2×10^{-1}	9.6×10^{-2}	$1.62\times10^{-3}a^{-5}$	6.25×10^{0}
2.5×10^{-1}	16.4×10^{-2}		2.72×10^{-1}
5.0×10^{-1}	33.6×10^{-2}		1.74×10^{-2}
1.0×10^{0}	66.4×10^{-2}		1.08×10^{-3}
3.1×10^{0}	3.536×10^{0}		2.00×10^{-5}
1.0×10^{1}	10.264×10^{0}		1.66×10^{-7}

*This is classified data. Each interval is symmetric about the listed diameter. They are unequal in order to fit the breaks in the Sekanina-Miller distribution function and for convenience in calculation.

Table 10

Sekanina-Miller Distribution Function Decades of Mass

Mass (g)	Diameter (cm) (ρ=1g cm^{-3})	Dist. Func. n(a) (#cm^{-1}g^{-1})	Interval Δa(cm)	Norm. Dist. n(a)Δa (#g^{-1})
4.19×10^{-12}*	10^{-4}	6.900×10^{14}	1.773×10^{-4}#	1.223×10^{11}
3×10^{-11}	3.855×10^{-4}	2.395×10^{13}	3.086×10^{-4}	7.391×10^{9}
3×10^{-10}	8.306×10^{-4}	9.455×10^{11}	6.648×10^{-4}	6.286×10^{8}
3×10^{-9}	1.789×10^{-3}	4.393×10^{10}	1.432×10^{-3}	6.291×10^{7}
3×10^{-8}	3.855×10^{-3}	2.038×10^{9}	3.086×10^{-3}	6.289×10^{6}
3×10^{-7}	8.306×10^{-3}	4.098×10^{7}	6.648×10^{-3}	2.724×10^{5}
3×10^{-6}	1.789×10^{-2}	8.840×10^{5}	1.432×10^{-2}	1.266×10^{4}
3×10^{-5}	3.855×10^{-2}	1.903×10^{4}	3.086×10^{-2}	5.873×10^{2}
3×10^{-4}	8.306×10^{-2}	4.098×10^{2}	6.648×10^{-2}	2.724×10^{1}
3×10^{-3}	1.789×10^{-1}	8.840×10^{0}	1.432×10^{-1}	1.266×10^{0}
3×10^{-2}	3.855×10^{-1}	1.903×10^{-1}	3.086×10^{-1}	5.873×10^{-2}
3×10^{-1}	8.306×10^{-1}	4.098×10^{-3}	6.648×10^{-1}	2.724×10^{-3}
3×10^{0}	1.789×10^{0}	8.840×10^{-5}	1.432×10^{0}	1.266×10^{-4}

* 3.05×10^{-12} - 1×10^{-11}

0.9×10^{-4} - 2.673×10^{-4}

Table 11

P/Tempel 2

Total Dust Production
at 1.6 AU Pre-perihelion
(number of particles s^{-1})

Particle Diameter (cm)	Extreme Low	Nominal	Extreme High
0.925×10^{-4}	3.14×10^{11}	3.10×10^{12}	8.55×10^{14}
0.975×10^{-4}	7.27×10^{11}	7.17×10^{12}	1.98×10^{15}
1.125×10^{-4}	1.07×10^{13}	1.05×10^{14}	2.90×10^{16}
1.500×10^{-4}	--	6.66×10^{13}	1.84×10^{16}
2.175×10^{-4}	--	4.05×10^{13}	1.12×10^{16}
3.3×10^{-4}	--	1.29×10^{13}	3.57×10^{15}
5.0×10^{-4}	--	3.51×10^{12}	9.69×10^{14}
9.0×10^{-4}	--	1.00×10^{12}	2.77×10^{14}
2.4×10^{-3}	--	7.95×10^{10}	2.19×10^{13}
4.7×10^{-3}	--	3.78×10^{9}	1.04×10^{12}
6.9×10^{-3}	--	5.56×10^{8}	1.53×10^{11}
1.0×10^{-2}	--	1.58×10^{8}	4.36×10^{10}
2.0×10^{-2}	--	1.97×10^{7}	5.45×10^{9}
5.0×10^{-2}	--	5.56×10^{5}	1.53×10^{8}
1.2×10^{-1}	--	1.52×10^{4}	4.21×10^{6}
2.5×10^{-1}	--	--	1.83×10^{5}
5.0×10^{-1}	--	--	1.71×10^{4}
1.0×10^{0}	--	--	7.27×10^{2}
3.1×10^{0}	--	--	1.35×10^{1}
1.0×10^{1}	--	--	1.12×10^{-1}
Total Mass Flow	2.474×10^{2} g s^{-1}	2.438×10^{3} g s^{-1}	6.731×10^{5} g s^{-1}

Table 12

P/Tempel 2 — Total Dust Production at 1.4 AU Post-perihelion (number of particles s^{-1})

Particle Diameter (cm)	Extreme Low	Nominal	Extreme High
0.925×10^{-4}	4.63×10^{12}	4.56×10^{13}	1.38×10^{16}
0.975×10^{-4}	1.07×10^{13}	1.06×10^{14}	3.19×10^{16}
1.125×10^{-4}	1.57×10^{14}	1.55×10^{15}	4.67×10^{17}
1.500×10^{-4}	9.95×10^{13}	9.80×10^{14}	2.96×10^{17}
2.175×10^{-4}	6.05×10^{13}	5.96×10^{14}	1.80×10^{17}
3.3×10^{-4}	1.94×10^{13}	1.91×10^{14}	5.76×10^{16}
5.0×10^{-4}	5.25×10^{12}	5.17×10^{13}	1.56×10^{16}
9.0×10^{-4}	1.50×10^{12}	1.48×10^{13}	4.46×10^{15}
2.4×10^{-3}	--	1.17×10^{12}	3.53×10^{14}
4.7×10^{-3}	--	5.56×10^{10}	1.68×10^{13}
6.9×10^{-3}	--	8.18×10^{9}	2.47×10^{12}
1.0×10^{-2}	--	2.32×10^{9}	7.02×10^{11}
2.0×10^{-2}	--	2.91×10^{8}	8.78×10^{10}
5.0×10^{-2}	--	8.18×10^{6}	2.47×10^{9}
1.2×10^{-1}	--	2.24×10^{5}	6.78×10^{7}
2.5×10^{-1}	--	9.76×10^{3}	2.95×10^{6}
5.0×10^{-1}	--	6.24×10^{2}	1.89×10^{5}
1.0×10^{0}	--	3.88×10^{1}	1.17×10^{4}
3.1×10^{0}	--	--	2.17×10^{2}
1.0×10^{1}	--	--	1.80×10^{0}
2.0×10^{1}	--	--	5.34×10^{-2}
Total Mass Flow	3.645×10^{3} g s^{-1}	3.589×10^{4} g s^{-1}	1.084×10^{7} g s^{-1}

Table 13

P/Tempel 2

Total Dust Production
at 1.8 AU Post-perihelion
(number of particles s^{-1})

Particle Diameter (cm)	Extreme Low	Nominal	Extreme High
0.925×10^{-4}	1.05×10^{12}	1.03×10^{13}	2.85×10^{15}
0.975×10^{-4}	2.42×10^{12}	2.39×10^{13}	6.61×10^{15}
1.125×10^{-4}	3.55×10^{13}	3.50×10^{14}	9.69×10^{16}
1.500×10^{-4}	2.25×10^{13}	2.22×10^{14}	6.14×10^{16}
2.175×10^{-4}	1.37×10^{13}	1.35×10^{14}	3.73×10^{16}
3.3×10^{-4}	4.38×10^{12}	4.31×10^{13}	1.19×10^{16}
5.0×10^{-4}	--	1.17×10^{13}	3.24×10^{15}
9.0×10^{-4}	--	3.34×10^{12}	9.24×10^{14}
2.4×10^{-3}	--	2.65×10^{11}	7.33×10^{13}
4.7×10^{-3}	--	1.26×10^{10}	3.48×10^{12}
6.9×10^{-3}	--	1.85×10^{9}	5.13×10^{11}
1.0×10^{-2}	--	5.27×10^{8}	1.46×10^{11}
2.0×10^{-2}	--	6.58×10^{7}	1.82×10^{10}
5.0×10^{-2}	--	1.85×10^{6}	5.13×10^{8}
1.2×10^{-1}	--	5.08×10^{4}	1.40×10^{7}
2.5×10^{-1}	--	2.21×10^{3}	6.11×10^{5}
5.0×10^{-1}	--	--	3.91×10^{4}
1.0×10^{0}	--	--	2.43×10^{3}
3.1×10^{0}	--	--	4.50×10^{1}
1.0×10^{1}	--	--	3.73×10^{-1}
Total Mass Flow	8.247×10^{2} g s^{-1}	8.126×10^{3} g s^{-1}	2.248×10^{6} g s^{-1}

Table 14

P/Tempel 2

Total Dust Production
at 2.2 AU Post-perihelion
(number of particles s^{-1})

Particle Diameter (cm)	Extreme Low	Nominal	Extreme High
0.925×10^{-4}	--	1.21×10^{12}	3.34×10^{14}
0.975×10^{-4}	--	2.81×10^{12}	7.73×10^{14}
1.125×10^{-4}	--	4.12×10^{13}	1.13×10^{16}
1.500×10^{-4}	--	2.61×10^{13}	7.17×10^{15}
2.175×10^{-4}	--	1.59×10^{13}	4.36×10^{15}
3.3×10^{-4}	--	5.07×10^{12}	1.40×10^{15}
5.0×10^{-4}	--	1.38×10^{12}	3.78×10^{14}
9.0×10^{-4}	--	3.92×10^{11}	1.08×10^{14}
2.4×10^{-3}	--	3.11×10^{10}	8.57×10^{12}
4.7×10^{-3}	--	1.48×10^{9}	4.07×10^{11}
6.9×10^{-3}	--	2.18×10^{8}	5.99×10^{10}
1.0×10^{-2}	--	6.19×10^{7}	1.70×10^{10}
2.0×10^{-2}	--	7.73×10^{6}	2.13×10^{9}
5.0×10^{-2}	--	--	5.99×10^{7}
1.2×10^{-1}	--	--	1.64×10^{6}
2.5×10^{-1}	--	--	7.15×10^{4}
5.0×10^{-1}	--	--	4.57×10^{3}
1.0×10^{0}	--	--	2.84×10^{2}
3.1×10^{0}	--	--	5.26×10^{0}
1.0×10^{1}	--	--	4.36×10^{-2}
Total Mass Flow	--	9.549×10^{2} g s^{-1}	2.628×10^{5} g s^{-1}

Table 15

P/Tempel 2 — Near Nucleus Dust Parameters at 1.6 AU Pre-perihelion

Particle Diameter (cm)	Extreme Low Model: Particle Density# at 10^2 km (m^{-3})	Extreme Low Model: Particle Flux# at 10^2 km ($m^{-2}\ s^{-1}$)	Nominal Model: Particle Density* at 10^2 km (m^{-3})	Nominal Model: Particle Flux* at 10^2 km ($m^{-2}\ s^{-1}$)	Extreme High Model: Particle Density† at 10^2 km (m^{-3})	Extreme High Model: Particle Flux† at 10^2 km ($m^{-2}\ s^{-1}$)
0.925×10^{-4}	1.32×10^{0}	2.50×10^{0}	3.93×10^{0}	3.68×10^{2}	6.43×10^{1}	2.54×10^{4}
0.975×10^{-4}	3.68×10^{0}	5.79×10^{2}	9.35×10^{0}	8.51×10^{2}	1.52×10^{2}	5.88×10^{4}
1.125×10^{-4}	1.18×10^{2}	8.51×10^{1}	1.47×10^{2}	1.25×10^{4}	2.28×10^{3}	8.61×10^{5}
1.500×10^{-4}	--		1.09×10^{2}	7.91×10^{3}	1.56×10^{3}	5.46×10^{5}
2.175×10^{-4}	--		8.00×10^{1}	4.81×10^{3}	1.01×10^{3}	3.33×10^{5}
3.3×10^{-4}	--		3.17×10^{1}	1.53×10^{3}	3.59×10^{2}	1.06×10^{5}
5.0×10^{-4}	--		1.08×10^{1}	4.17×10^{2}	1.06×10^{2}	2.88×10^{4}
9.0×10^{-4}	--		4.21×10^{0}	1.19×10^{2}	3.32×10^{1}	8.22×10^{3}
2.4×10^{-3}	--		5.83×10^{-1}	9.44×10^{0}	3.63×10^{0}	6.50×10^{2}
4.7×10^{-3}	--		4.16×10^{-2}	4.49×10^{-1}	2.19×10^{-1}	3.09×10^{1}
6.9×10^{-3}	--		7.77×10^{-3}	6.60×10^{-2}	3.52×10^{-2}	4.54×10^{0}
1.0×10^{-2}	--		2.84×10^{-3}	1.88×10^{-2}	1.14×10^{-2}	1.29×10^{0}
2.0×10^{-2}	--		6.00×10^{-4}	2.34×10^{-3}	1.89×10^{-3}	1.62×10^{-1}
5.0×10^{-2}	--		4.40×10^{-5}	6.60×10^{-5}	8.54×10^{-5}	4.54×10^{-3}
1.2×10^{-1}	--		1.80×10^{-4}	1.81×10^{-6}	3.74×10^{-6}	1.25×10^{-4}
2.5×10^{-1}	--		--	--	2.44×10^{-7}	5.43×10^{-6}
5.0×10^{-1}	--		--	--	3.39×10^{-8}	5.08×10^{-7}
1.0×10^{0}	--		--	--	2.20×10^{-9}	2.16×10^{-8}
3.1×10^{0}	--		--	--	9.11×10^{-11}	4.01×10^{-10}
1.0×10^{1}	--		--	--	2.56×10^{-12}	3.33×10^{-12}
Largest escaping particle diameter (cm)				1.21×10^{-1}		2.20×10^{1}

#Isotropically

*Within 60° cone

†Within 120° cone

Table 16

P/Tempel 2 Near Nucleus Dust Parameters at 1.4 AU Post-perihelion

Particle Diameter (cm)	Extreme Low Model: Particle Density[#] at 10^2 km (m^{-3})	Extreme Low Model: Particle Flux[#] at 10^2 km (m^{-2} s^{-1})	Nominal Model: Particle Density[*] at 10^2 km (m^{-3})	Nominal Model: Particle Flux[*] at 10^2 km (m^{-2} s^{-1})	Extreme High Model: Particle Density[†] at 10^2 km (m^{-3})	Extreme High Model: Particle Flux[†] at 10^2 km (m^{-2} s^{-1})
0.925×10^{-4}	9.75×10^{-1}	3.68×10^{1}	1.91×10^{1}	5.42×10^{3}	1.01×10^{3}	4.10×10^{5}
0.975×10^{-4}	2.33×10^{0}	8.51×10^{1}	4.53×10^{1}	1.26×10^{4}	2.40×10^{3}	9.47×10^{5}
1.125×10^{-4}	3.76×10^{1}	1.25×10^{3}	7.00×10^{2}	1.84×10^{5}	3.60×10^{4}	1.39×10^{7}
1.500×10^{-4}	2.90×10^{1}	7.92×10^{2}	4.81×10^{2}	1.16×10^{5}	2.33×10^{4}	8.79×10^{6}
2.175×10^{-4}	2.30×10^{1}	4.81×10^{2}	3.45×10^{2}	7.08×10^{4}	1.52×10^{4}	5.34×10^{6}
3.3×10^{-4}	1.04×10^{1}	1.54×10^{2}	1.27×10^{2}	2.27×10^{4}	5.34×10^{3}	1.71×10^{6}
5.0×10^{-4}	4.14×10^{0}	4.18×10^{1}	4.07×10^{1}	6.14×10^{3}	1.59×10^{3}	4.63×10^{5}
9.0×10^{-4}	2.49×10^{0}	1.19×10^{1}	1.49×10^{1}	1.76×10^{3}	5.09×10^{2}	1.32×10^{5}
2.4×10^{-3}	--	--	1.99×10^{0}	1.39×10^{2}	5.21×10^{1}	1.05×10^{4}
4.7×10^{-3}	--	--	1.34×10^{-1}	6.60×10^{0}	3.06×10^{0}	4.99×10^{2}
6.9×10^{-3}	--	--	2.42×10^{-2}	9.72×10^{-1}	5.31×10^{-1}	7.33×10^{1}
1.0×10^{-2}	--	--	8.40×10^{-3}	2.76×10^{-1}	1.74×10^{-1}	2.08×10^{1}
2.0×10^{-2}	--	--	1.54×10^{-3}	3.46×10^{-2}	2.66×10^{-2}	2.61×10^{0}
5.0×10^{-2}	--	--	7.36×10^{-5}	9.72×10^{-4}	1.20×10^{-3}	7.33×10^{-2}
1.2×10^{-1}	--	--	3.50×10^{-6}	2.66×10^{-5}	5.23×10^{-5}	2.01×10^{-3}
2.5×10^{-1}	--	--	2.63×10^{-7}	1.16×10^{-6}	3.40×10^{-6}	8.76×10^{-5}
5.0×10^{-1}	--	--	3.09×10^{-8}	7.41×10^{-8}	3.21×10^{-7}	5.61×10^{-6}
1.0×10^{0}	--	--	5.12×10^{-9}	4.61×10^{-9}	2.99×10^{-8}	3.47×10^{-7}
3.1×10^{0}	--	--	--	--	1.19×10^{-9}	6.44×10^{-9}
1.9×10^{1}	--	--	--	--	2.97×10^{-11}	5.34×10^{-11}
2.0×10^{1}	--	--	--	--	3.17×10^{-12}	1.59×10^{-12}
Largest escaping particle diameter (cm)		1.9×10^{-1}		1.8×10^{0}		2.9×10^{1}

[#]Isotropically

[*]Within 60° cone

[†]Within 120° cone

ORIGINAL PAGE IS OF POOR QUALITY

Table 17

P/Tempel 2 — Near Nucleus Dust Parameters at 1.8 AU Post-perihelion

Particle Diameter (cm)	Extreme Low Model: Particle Density# at 10^2 km (m^{-3})	Extreme Low Model: Particle Flux# at 10^2 km ($m^{-2}\ s^{-1}$)	Nominal Model: Particle Density* at 10^2 km (m^{-3})	Nominal Model: Particle Flux* at 10^2 km ($m^{-2}\ s^{-1}$)	Extreme High Model: Particle Density† at 10^2 km (m^{-3})	Extreme High Model: Particle Flux† at 10^2 km ($m^{-2}\ s^{-1}$)
0.925×10^{-4}	6.79×10^{-1}	8.36×10^{0}	7.07×10^{0}	1.22×10^{3}	2.24×10^{2}	8.46×10^{4}
0.975×10^{-4}	1.65×10^{0}	1.93×10^{1}	1.69×10^{1}	2.84×10^{3}	5.28×10^{2}	1.96×10^{5}
1.125×10^{-4}	2.77×10^{1}	2.82×10^{2}	2.65×10^{2}	4.16×10^{4}	7.90×10^{3}	2.88×10^{6}
1.500×10^{-4}	2.42×10^{1}	1.79×10^{2}	1.95×10^{2}	2.64×10^{4}	5.43×10^{3}	1.82×10^{6}
2.175×10^{-4}	2.54×10^{1}	1.09×10^{2}	1.43×10^{2}	1.60×10^{4}	3.46×10^{3}	1.11×10^{6}
3.3×10^{-4}	2.32×10^{1}	3.49×10^{1}	5.66×10^{1}	5.12×10^{3}	1.20×10^{3}	3.53×10^{5}
5.0×10^{-4}	--	--	1.90×10^{1}	1.39×10^{3}	3.58×10^{2}	9.62×10^{4}
9.0×10^{-4}	--	--	7.39×10^{0}	3.97×10^{2}	1.19×10^{2}	2.74×10^{4}
2.4×10^{-3}	--	--	9.89×10^{-1}	3.15×10^{1}	1.30×10^{1}	2.18×10^{3}
4.7×10^{-3}	--	--	6.80×10^{-2}	1.50×10^{0}	8.01×10^{-1}	1.03×10^{2}
6.9×10^{-3}	--	--	1.24×10^{-2}	2.20×10^{-1}	1.32×10^{-1}	1.52×10^{1}
1.0×10^{-2}	--	--	4.41×10^{-3}	6.26×10^{-2}	4.38×10^{-2}	4.34×10^{0}
2.0×10^{-2}	--	--	8.40×10^{-4}	7.82×10^{-3}	7.13×10^{-3}	5.40×10^{-1}
5.0×10^{-2}	--	--	4.48×10^{-5}	2.20×10^{-4}	3.25×10^{-4}	1.52×10^{-2}
1.2×10^{-1}	--	--	2.74×10^{-6}	6.03×10^{-6}	1.42×10^{-5}	4.16×10^{-4}
2.5×10^{-1}	--	--	3.75×10^{-7}	2.62×10^{-7}	9.30×10^{-7}	1.81×10^{-5}
5.0×10^{-1}	--	--	--	--	8.93×10^{-8}	1.16×10^{-6}
1.0×10^{0}	--	--	--	--	8.59×10^{-9}	7.21×10^{-8}
3.1×10^{0}	--	--	--	--	3.71×10^{-10}	1.34×10^{-9}
1.0×10^{1}	--	--	--	--	1.38×10^{-11}	1.11×10^{-11}
Largest escaping particle diameter (cm)		4.26×10^{-4}		4.05×10^{-1}		1.74×10^{1}

#Isotropically

*Within 60° cone

†Within 120° cone

Table 18

P/Tempel 2 — Near Nucleus Dust Parameters at 2.2 AU Post-perihelion

Particle Diameter (cm)	Extreme Low Model: Particle Density# at 10^2 km (m^{-3})	Extreme Low Model: Particle Flux# at 10^2 km (m^{-2} s^{-1})	Nominal Model: Particle Density* at 10^2 km (m^{-3})	Nominal Model: Particle Flux* at 10^2 km (m^{-2} s^{-1})	Extreme High Model: Particle Density† at 10^2 km (m^{-3})	Extreme High Model: Particle Flux† at 10^2 km (m^{-2} s^{-1})
0.925×10^{-4}	--	--	2.50×10^{0}	1.44×10^{2}	2.86×10^{1}	9.92×10^{3}
0.975×10^{-4}	--	--	5.96×10^{0}	3.34×10^{2}	6.69×10^{1}	2.30×10^{4}
1.125×10^{-4}	--	--	9.41×10^{1}	4.89×10^{3}	1.01×10^{3}	3.36×10^{5}
1.500×10^{-4}	--	--	6.95×10^{1}	3.10×10^{3}	6.65×10^{2}	2.13×10^{5}
2.175×10^{-4}	--	--	5.16×10^{1}	1.89×10^{3}	4.39×10^{2}	1.29×10^{5}
3.3×10^{-4}	--	--	2.06×10^{1}	6.02×10^{2}	1.55×10^{2}	4.16×10^{4}
5.0×10^{-4}	--	--	7.06×10^{0}	1.64×10^{2}	4.54×10^{1}	1.12×10^{4}
9.0×10^{-4}	--	--	2.80×10^{0}	4.66×10^{1}	1.58×10^{1}	3.21×10^{3}
2.4×10^{-3}	--	--	4.06×10^{-1}	3.68×10^{0}	1.72×10^{0}	2.54×10^{2}
4.7×10^{-3}	--	--	3.03×10^{-2}	1.76×10^{-1}	1.03×10^{-1}	1.21×10^{1}
6.9×10^{-3}	--	--	6.02×10^{-3}	2.59×10^{-2}	1.78×10^{-2}	1.78×10^{0}
1.0×10^{-2}	--	--	2.37×10^{-3}	7.35×10^{-3}	5.72×10^{-3}	5.05×10^{-1}
2.0×10^{-2}	--	--	6.56×10^{-4}	9.18×10^{-4}	1.03×10^{-3}	6.32×10^{-2}
5.0×10^{-2}	--	--	--	--	4.69×10^{-5}	1.78×10^{-3}
1.2×10^{-1}	--	--	--	--	2.07×10^{-6}	4.87×10^{-5}
2.5×10^{-1}	--	--	--	--	1.37×10^{-7}	2.12×10^{-6}
5.0×10^{-1}	--	--	--	--	1.33×10^{-8}	1.36×10^{-7}
1.0×10^{0}	--	--	--	--	1.32×10^{-9}	8.43×10^{-9}
1.1×10^{0}	--	--	--	--	6.25×10^{-11}	1.56×10^{-10}
1.0×10^{1}	--	--	--	--	6.47×10^{-12}	1.29×10^{-12}
Largest escaping particle diameter (cm)		4.99×10^{-5}		4.75×10^{-2}	1.17×10^{1}	

#Isotropically

*Within 60° cone

†Within 120° cone

Table 19

P/Tempel 2 — Dust Envelope Apex Distance at 1.6 AU Pre-perihelion

Particle Diameter (cm)	Apex Distance (km) Low Model	Nominal	High Model
0.925×10^{-4}	3.05×10^{-1}	1.49×10^{3}	5.32×10^{4}
0.975×10^{-4}	2.22×10^{-1}	1.49×10^{3}	5.36×10^{4}
1.125×10^{-4}	5.38×10^{-2}	1.49×10^{3}	5.90×10^{4}
1.500×10^{-4}	--	1.47×10^{3}	6.82×10^{4}
2.175×10^{-4}	--	1.45×10^{3}	8.63×10^{4}
3.3×10^{-4}	--	1.42×10^{3}	1.06×10^{5}
5.0×10^{-4}	--	1.38×10^{3}	1.36×10^{5}
9.0×10^{-4}	--	1.32×10^{3}	2.04×10^{5}
2.4×10^{-3}	--	1.16×10^{3}	2.84×10^{5}
4.7×10^{-3}	--	1.01×10^{3}	3.45×10^{5}
6.9×10^{-3}	--	9.19×10^{2}	4.24×10^{5}
1.0×10^{-2}	--	8.03×10^{2}	4.79×10^{5}
5.0×10^{-2}	--	2.07×10^{2}	5.22×10^{5}
1.2×10^{-1}	--	<1	4.94×10^{5}
5.0×10^{-1}	--	--	4.15×10^{5}
1.0×10^{0}	--	--	3.54×10^{5}
3.1×10^{0}	--	--	2.21×10^{5}
1.0×10^{1}	--	--	6.23×10^{4}
Largest Apex (km)	<1	1500	550,000

Table 20

P/Tempel 2 Dust Envelope Apex Distance at 1.4 AU Post-perihelion

Particle Diameter (cm)	Apex Distance (km) Low Model	Nominal	High Model
0.925×10^{-4}	9.33×10^{1}	1.05×10^{4}	4.26×10^{4}
0.975×10^{-4}	9.17×10^{1}	1.06×10^{4}	4.27×10^{4}
1.125×10^{-4}	8.76×10^{1}	1.10×10^{4}	4.71×10^{4}
1.500×10^{-4}	7.89×10^{1}	1.24×10^{4}	6.02×10^{4}
2.175×10^{-4}	6.70×10^{1}	1.29×10^{4}	7.57×10^{4}
3.3×10^{-4}	5.17×10^{1}	1.49×10^{4}	9.54×10^{4}
5.0×10^{-4}	3.60×10^{1}	1.61×10^{4}	1.20×10^{5}
9.0×10^{-4}	1.46×10^{1}	1.77×10^{4}	1.72×10^{5}
2.4×10^{-3}	--	1.66×10^{4}	2.74×10^{5}
4.7×10^{-3}	--	1.61×10^{4}	3.53×10^{5}
6.9×10^{-3}	--	1.57×10^{4}	3.71×10^{5}
1.0×10^{-2}	--	1.52×10^{4}	4.07×10^{5}
5.0×10^{-2}	--	1.23×10^{4}	5.27×10^{5}
1.2×10^{-1}	--	9.79×10^{3}	5.02×10^{5}
5.0×10^{-1}	--	4.07×10^{3}	4.32×10^{5}
1.0×10^{0}	--	1.14×10^{3}	3.80×10^{5}
3.1×10^{0}	--	--	2.55×10^{5}
1.0×10^{1}	--	--	9.15×10^{4}
Largest Apex (km)	~100	18,000	550,000

Table 21

P/Tempel 2 — Dust Envelope Apex Distance at 1.8 AU Post-perihelion

Particle Diameter (cm)	Apex Distance (km) Low Model	Nominal	High Model
0.925×10^{-4}	1.63×10^{1}	6.46×10^{3}	6.14×10^{4}
0.975×10^{-4}	1.55×10^{1}	6.42×10^{3}	6.30×10^{4}
1.125×10^{-4}	1.36×10^{1}	6.47×10^{3}	6.96×10^{4}
1.500×10^{-4}	9.59×10^{0}	6.38×10^{3}	7.91×10^{4}
2.175×10^{-4}	4.69×10^{0}	6.37×10^{3}	1.04×10^{5}
3.3×10^{-4}	8.67×10^{-1}	6.31×10^{3}	1.34×10^{5}
5.0×10^{-4}	--	6.22×10^{3}	1.69×10^{5}
9.0×10^{-4}	--	6.06×10^{3}	2.24×10^{5}
2.4×10^{-3}	--	5.70×10^{3}	3.12×10^{5}
4.7×10^{-3}	--	5.31×10^{3}	3.65×10^{5}
6.9×10^{-3}	--	5.04×10^{3}	4.26×10^{5}
1.0×10^{-2}	--	4.71×10^{3}	4.58×10^{5}
5.0×10^{-2}	--	2.80×10^{3}	5.13×10^{5}
1.2×10^{-1}	--	1.36×10^{3}	4.81×10^{5}
5.0×10^{-1}	--	--	3.94×10^{5}
1.0×10^{0}	--	--	3.29×10^{5}
3.1×10^{0}	--	--	1.88×10^{5}
1.0×10^{1}	--	--	2.99×10^{4}
Largest Apex (km)	~20	6500	540,000

Table 22

P/Tempel 2 — Dust Envelope Apex Distance at 2.2 AU Post-perihelion

Particle Diameter (cm)	Apex Distance (km) Low Model	Nominal	High Model
0.925×10^{-4}	--	1.07×10^{3}	7.77×10^{4}
0.975×10^{-4}	--	1.07×10^{3}	8.00×10^{4}
1.125×10^{-4}	--	1.06×10^{3}	8.65×10^{4}
1.500×10^{-4}	--	1.04×10^{3}	1.07×10^{5}
2.175×10^{-4}	--	1.02×10^{3}	1.32×10^{5}
3.3×10^{-4}	--	9.81×10^{2}	1.67×10^{5}
5.0×10^{-4}	--	9.38×10^{2}	2.13×10^{5}
9.0×10^{-4}	--	8.65×10^{2}	2.59×10^{5}
2.4×10^{-3}	--	6.93×10^{2}	3.67×10^{5}
4.7×10^{-3}	--	5.51×10^{2}	4.49×10^{5}
6.9×10^{-3}	--	4.45×10^{2}	4.81×10^{5}
1.0×10^{-2}	--	3.35×10^{2}	5.43×10^{5}
5.0×10^{-2}	--	--	5.01×10^{5}
1.2×10^{-1}	--	--	4.62×10^{5}
5.0×10^{-1}	--	--	3.63×10^{5}
1.0×10^{0}	--	--	2.86×10^{5}
3.1×10^{0}	--	--	1.35×10^{5}
1.0×10^{1}	--	--	2.79×10^{3}
Largest Apex (km)	--	1070	545,000

Table 23

P/Tempel 2 Density of H_2O* vs Distance from Nucleus for Nominal Models

Distance from nucleus (km)	Heliocentric Distance (AU)			
	Pre-Perihelion	Post-Perihelion		
	1.6	1.4	1.8	2.2
Surface	1.23×10^{11}	1.82×10^{12}	4.11×10^{11}	4.83×10^{10}
1×10^{2}	1.58×10^{7}	2.33×10^{8}	5.27×10^{7}	6.19×10^{6}
2×10^{2}	3.31×10^{6}	4.86×10^{7}	1.10×10^{7}	1.30×10^{6}
5×10^{2}	4.11×10^{5}	6.03×10^{6}	1.37×10^{6}	1.62×10^{5}
1×10^{3}	9.04×10^{4}	1.32×10^{6}	3.02×10^{5}	3.57×10^{4}
2×10^{3}	2.21×10^{4}	3.21×10^{5}	7.42×10^{4}	6.82×10^{3}
5×10^{3}	3.30×10^{3}	4.68×10^{4}	1.12×10^{4}	1.36×10^{3}
1×10^{4}	7.34×10^{2}	1.01×10^{4}	2.56×10^{3}	3.20×10^{2}
2×10^{4}	1.45×10^{2}	1.86×10^{3}	5.33×10^{2}	7.07×10^{1}
5×10^{4}	1.16×10^{1}	1.19×10^{2}	4.92×10^{1}	7.82×10^{0}
Surface Pressure in active cone (dynes cm^{-2})	3.2×10^{-3}	4.6×10^{-2}	1.0×10^{-2}	1.2×10^{-3}

* molecules cm^{-3}

NASA–JPL–Coml, L.A., Calif